N87-22206

ROTORDYNAMIC COEFFICIENTS AND LEAKAGE FLOW OF PARALLEL GROOVED SEALS AND SMOOTH SEALS

R. Nordmann, F.J. Dietzen, and W. Janson
University of Kaiserslautern
German Federal Republic

A. Frei and S. Florjancic
Sulzer Brothers
Winterthur, Switzerland

Based on Childs finite length solution (ref. 1) for annular plain seals an extension of the bulk flow theory is derived to calculate the rotordynamic coefficients and the leakage flow of seals with parallel grooves in the stator. Hirs turbulent lubricant equations are modified to account for the different friction factors in circumferential and axial direction. Furthermore an average groove depth is introduced to consider the additional circumferential flow in the grooves. Theoretical and experimental results are compared for the smooth constant clearance seal and the corresponding seal with parallel grooves. Compared to the smooth seal the direct and cross-coupled stiffness coefficients as well as the direct damping coefficients are lower in the grooved seal configuration. Leakage is reduced by the grooving pattern.

INTRODUCTION

An important assumption for the reliability of high speed centrifugal pumps is a good rotordynamic behavior. Connected to this problem hydraulic forces acting on the rotor are of major importance. It is well known that neck or wear-ring seals as well as interstage seals (fig. 1) may have a large influrence on the bending vibrations of a pump rotor. Besides their designed function of reducing the leakage flow between the impeller outlet and inlet or two adjacent pump stages, respectively, the contactless seals have the potential to develop significant forces. This type of forces created by lateral rotor vibrations can be described by stiffness-, damping- and mass coefficients in a linearized model

$$\begin{bmatrix} F_x \\ F_y \end{bmatrix} = \begin{bmatrix} M & m \\ -m & M \end{bmatrix} \cdot \begin{bmatrix} \ddot{x} \\ \ddot{y} \end{bmatrix} + \begin{bmatrix} C & c \\ -c & C \end{bmatrix} \cdot \begin{bmatrix} \dot{x} \\ \dot{y} \end{bmatrix} + \begin{bmatrix} K & k \\ -k & K \end{bmatrix} \cdot \begin{bmatrix} x \\ y \end{bmatrix} \qquad (1)$$

For rotordynamic calculations of multistage pumps the machine designer needs to know this dynamic characteristics of the actual seal configuration. For smooth seals, where both stator and rotor elements have the same smooth surfaces, analytical and experimental investigations have been carried out (ref. 1,3,4,5). The results confirm the validity of equation (1) and dynamic coefficients can be predicted by the finite length solution derived in ref. 1 with sufficient accuracy. A finite length solution is also available for seals with different but directionally-homogeneous

surface roughness for the rotor and stator elements (ref. 2).

The subject of this investigation is a seal type with parallel grooves in the stator element and a smooth surface in the rotor element. Concerning the leakage flow, this type of seal is more effective than the pure smooth seal, because of higher friction in the axial direction. However, if pump rotordynamics is important the dynamic seal coefficients have to be known. Up to now the stiffness and damping characteristics of grooved seals and their influence to the stability and unbalance response of pump rotors is not well investigated and there is a need for additional research in this area.

At the present time, there are only a few techniques available in the technical literature. Black and Cochrane (ref. 6) have improved their earlier theory for smooth seals by introducing an equivalent length for the grooved section to reduce the circumferential pressure gradients. Recently, Childs and Kim (ref. 7) have extended their analysis procedure (ref. 2) to predict rotordynamic coefficients of grooved turbulent annular seals.

In the present paper an extension of the bulk flow theory (ref. 1) is given, to calculate rotordynamic coefficients and leakage for seals with parallel grooves in the stator. The theoretical results obtained by the developed procedure are correlated to experimental results, measured at a seal test rig. Furthermore the grooved seal results are compared with corresponding data of the smooth seal configuration.

BULK FLOW MODEL FOR SEALS WITH PARALLEL GROOVES

Seal geometry

Fig. 2 shows the type of seal, which is considered in our investigation. It consists of a smooth rotor and a circumferentially grooved stator. The seal has the radius R, the length L and may have different clearances at the entrance C_0 and the exit C_1, respectively. The groove geometry is described by the groove depth H_R and the groove length L_G and land length L_L. We assume, that the groove depth H_R has approximately the same order of magnitude as the seal clearances C_0, C_1.
In the following derivations the groove geometry is described simply by an average value H_R^* for the groove depth (fig. 2).

Bulk flow velocities

In Childs finite length analysis (ref. 1) for plain seals a bulk flow model was used. Following this procedure we introduce the bulk flow velocities U_Z in the axial Z-direction and U_Θ in the circumferential direction. The axial velocity U_Z is considered only in the region of the actual seal clearance H. Although there is a fluid circulation in the grooves: in the Z-direction, this part of the flow is neglected in our model (fig. 3). In circumferential direction the real velocity distribution (fig. 3) is replaced by a constant bulk flow U_Θ, which is assumed to act in the area of the average seal clearance $H^* = H + H_R^*$. At the rotor surface the fluid velocity is $R\omega$ with the shaft angular velocity ω.

Fig. 4 points out the variables of the bulk flow model for a seal location with coordinates Z and Θ: the two mentioned velocities U_Z, U_Θ, the fluid pressure p and

the local clearances H, $H^* = H + H_R^*$. All quantities depend on the coordinates Z and Θ and the time t, as well.

Wall shear stresses

Concerning the wall shear stresses at the rotor and the stator we refer to Hirs formulation, expressing the shear stresses by an empirical function of the bulk flow velocity relative to the wall. First we apply this relation for the rotor assuming a smooth surface in the two directions. With the bulk flow velocity $V_R=[(U_\Theta-R\omega)^2 + U_Z^2]^{1/2}$ relative to the rotor surface (fig. 5), we obtain

$$\tau_R = n_R \left(\frac{2H\ V_R}{\nu}\right)^{m_R} \frac{\rho}{2} V_R^2 = C_R \frac{\rho}{2} V_R^2 \qquad (2)$$

n_R, m_R are empirical turbulence coefficients, ρ is the fluid density and ν the kinematic viscosity of the fluid.
With the relations of figure 5 we can determine the components of the rotor wall shear stress

$$\tau_{R\Theta} = \tau_R (U_\Theta - R\omega)/V_R \quad ; \quad \tau_{RZ} = \tau_R\ U_Z/V_R \qquad (3)$$

Contrary to the definition of $\tau_{R\Theta}$ in equation (3) we use a slightly different form and define $\tau_{R\Theta}$ with the seal clearance H^* instead of H, which is used for τ_{RZ} in the axial direction. After some steps we obtain from equations (2) and (3)

$$\tau_{R\Theta} = \frac{n_R}{2} \rho\ U_Z\ (U_\Theta - R\omega)\ \left(\frac{H^*}{H}\right)^{m_R} R_a^{m_R} \left\{1 + \left(\frac{U_\Theta - R\omega}{U_Z}\right)^2\right\}^{(1+m_R)/2} \qquad (4a)$$

$$\tau_{RZ} = \frac{n_R}{2} \rho\ U_Z^2\ R_a^{m_R} \left\{1 + \left(\frac{U_\Theta - R\omega}{U_Z}\right)^2\right\}^{(1+m_R)/2} \qquad (4b)$$

with the axial Reynolds number $R_a = \frac{2H\ U_Z}{\nu}$.

Caused by the parallel grooves the stator has different friction characteristics in the two directions. In axial direction it behaves like a rough surface. For the circumferential direction we assume a smooth surface. Again we refer to Hirs formulation and express the wall shear stress τ_s in dependence of the bulk flow velocity $V_S = (U_\Theta^2 + U_Z^2)^{1/2}$

$$\tau_S = C_S \frac{\rho}{2} V_S^2 \qquad (5)$$

In the case of the grooved stator the triangle ratios of figure 5 are not quite correct. Nevertheless, we still use the relations and express the shear stress components approximately by

$$\tau_{S\Theta} = \tau_S\ U_\Theta/V_S \quad ; \quad \tau_{SZ} = \tau_S\ U_Z/V_S \qquad (6)$$

The resultant friction factor C_S (eq. 5) can be introduced by the following superposition rule

$$C_S = (C_{S\Theta}^2 \cos^2\varphi + C_{SZ}^2 \sin^2\varphi)^{1/2}$$

$$C_{S\Theta} = n_{S\Theta} \left(\frac{2H^* V_S}{\nu}\right)^{m_{S\Theta}} \qquad (7)$$

$$C_{SZ} = n_{SZ} \left(\frac{2H\ V_S}{\nu}\right)^{m_{SZ}}$$

$n_{S\Theta}$, n_{SZ}, $m_{S\Theta}$, m_{SZ} are empirical turbulence coefficients.

Formula (7) describes the change of the resultant stator friction factor C_S in dependence of the local flow angle φ (figs. 5,6). If we consider one of the special cases, e.g. a pure flow in axial direction, we obtain

$$U_Z = V_S, \quad U_\Theta = 0, \quad \varphi = \pi/2, \quad \sin\varphi = 1, \quad \cos\varphi = 0$$

$$C_S = C_{SZ}, \quad \tau_{S\Theta} = 0, \quad \tau_{SZ} = C_{SZ} \frac{\rho}{2} U_Z^2 .$$

From equations (5), (6), (7) we finally end up with the two shear force components

$$\tau_{S\Theta} = C_S'' \left(\frac{H^*}{H}\right)^{m_{S\Theta}} \frac{n_{S\Theta}}{2} \rho\, U_Z\, U_\Theta\, R_a^{m_{S\Theta}} \left\{1 + \left(\frac{U_\Theta}{U_Z}\right)^2\right\}^{(1+m_{S\Theta})/2} \qquad (8a)$$

$$\tau_{SZ} = C_S' \frac{n_{SZ}}{2} \rho\, U_Z^2\, R_a^{m_{SZ}} \left\{1 + \left(\frac{U_\Theta}{U_Z}\right)^2\right\}^{(1+m_{SZ})/2} \qquad (8b)$$

C_S', C_S'' are defined in the Appendix. (8a) and (8b) can be compared with prior results from Childs and Kim (ref. 2). They differ only in the coefficients C_S', C_S''.

BULK FLOW MOMENTUM AND CONTINUITY EQUATIONS

Figures 7 and 8 show a differential element of the fluid having the dimensions $Rd\Theta$, dZ, $H(Z,\Theta,t)$ or $H^*(Z,\Theta,t)$ respectively. The upper and lower surfaces correspond to the rotor and stator seal elements and have the velocities $R\omega$ and zero. Figure 7 points out the bulk flow velocity components U_Z and U_Θ with their changes in axial and circumferential direction along the element. For the derivation of the momentum equations the wall shear stresses τ_s, τ_r and the pressure p at the different seal surfaces have to be taken in account (fig. 8). Summing forces in the two directions for the free body diagram leads to the axial and circumferential momentum equations 9 and 10, respectively

$$- H \frac{\partial p}{\partial Z} = \tau_{SZ}+\tau_{RZ} + \rho H \left(\frac{\partial U_Z}{\partial t} + U_Z \frac{\partial U_Z}{\partial Z} + U_\Theta \frac{\partial U_Z}{R\partial_\Theta}\right) - \rho H_R^* U_Z \frac{\partial U_\Theta}{R\partial_\Theta} = 0 \qquad (9)$$

$$- \frac{H^*}{R} \frac{\partial p}{\partial \Theta} = \tau_{S\Theta}+\tau_{R\Theta} + \rho H^* \left(\frac{\partial U_\Theta}{\partial t} + \frac{U_\Theta}{R} \frac{\partial U_\Theta}{\partial \Theta} + U_Z \frac{\partial U_\Theta}{\partial Z}\right) - \rho H_R^* U_Z \frac{\partial U_\Theta}{\partial Z} = 0 \qquad (10)$$

In comparison to the derivations of reference 2 both equations have an additional term with the average groove depth H_R^*, expressing an added momentum change caused by the grooves. Furthermore the shear stresses are different as described in equations (4) and (8). Note that H^* is used in the circumferential momentum equation.

The bulk flow continuity equation (11) also has

$$\frac{\partial H}{\partial t} + \frac{1}{R} \left(\frac{\partial HU_\Theta}{\partial \Theta}\right) + \left(\frac{\partial HU_Z}{\partial Z}\right) + \frac{1}{R} H_R^* \frac{\partial U_\Theta}{\partial \Theta} = 0 \qquad (11)$$

an added term resulting from the flow difference in circumferential direction in the area of the grooves. If we substitute the shear stresses τ_{SZ}, τ_{RZ}, $\tau_{S\Theta}$, $\tau_{R\Theta}$ by the velocity-dependent formulas (4) and (8) we obtain the complete bulk flow equations (see Appendix A), which can be used for further analysis. By introducing the following variables

$$u_z = U_z/\bar{V}, \quad u_\Theta = U_\Theta/R\omega, \quad \tilde{p} = p/\rho\bar{V}^2$$

$$h = H/\bar{C}, \quad \tau = t/T, \quad z = Z/L, \quad C = (C_o + C_1)/2$$

$$T = L/\bar{V}, \quad b = \bar{V}/R\omega, \quad \bar{V} \text{ average axial velocity}$$

the equations can be treated also in nondimensional form.

PERTURBATION ANALYSIS

In the further analysis we follow strictly ref. 2. The governing equation (9), (10), (11) or the corresponding equations in non-dimensional form define the bulk flow velocity components u_Θ, u_z and the pressure $\tilde{p}$ as a function of the variables $R\Theta$, z and the time τ. The expansion of this equations in the perturbation variables

$$\begin{aligned} u_z &= u_{zo} + \varepsilon u_{z1} & u_\Theta &= u_{\Theta o} + \varepsilon u_{\Theta 1} \\ h &= h_o + \varepsilon h_1 & \tilde{p} &= \tilde{p}_o + \varepsilon \tilde{p}_1 \end{aligned} \qquad (12)$$

with the eccentricity ratio $\varepsilon = e/\bar{C}$ yields zeroth-order and first-order perturbation equations.

Zeroth - Order - Equations

The eccentricity ratio $\varepsilon = 0$ describes the centered position of the rotor in the stator element. If we introduce u_{zo}, $u_{\theta o}$, h_o and p_o in the nondimensional bulk flow equations, we obtain the following zeroth order perturbation equations.
Axial Momentum Equation:

$$\frac{\partial \tilde{p}_o}{\partial z} = -\frac{1}{2f^3}\{\sigma_R\, a_{oR} + \sigma_{sz}\, a_{osz}\, De + 4q\} \tag{13a}$$

Circumferential Momentum Equation:

$$\frac{\partial u_{\theta o}}{\partial z} = -\frac{1}{2f}\left\{\left(\frac{h_o^*}{h_o}\right)^{m_R} \sigma_R\, a_{oR}\,(u_{\theta o}-1) + \left(\frac{h_o^*}{h_o}\right)^{m_{s\theta}} \sigma_{s\theta} a_{os\theta}\, Da\, u_{\theta o}\right\} \tag{13b}$$

Contuniity Equation:

$$u_{z\theta} = \frac{1}{h_o} \tag{13c}$$

The parameters of these equations are defined in Appendix B. $h_o = f$ is the dimensionless clearance function for the centered position and $q = (C_o - C_1)/(C_o + C_1)$ is a measure of the degree of taper in a seal. For the constant clearance seal, treated later in this paper, it follows $q = 0$ and $h_o = 1$. The quantities σ_R, σ_{sz} and $\sigma_{s\theta}$ are defined by

$$\sigma_R = \left(\frac{L}{\bar{C}}\right)\lambda_R \quad ; \quad \sigma_{sz} = \left(\frac{L}{\bar{C}}\right)\lambda_{sz}; \quad \sigma_{s\theta} = \left(\frac{L}{\bar{C}}\right)\lambda_{s\theta} \tag{14}$$

with the wall friction factors

$$\lambda_R = n_R\, R_{ao}^{m_R}\left(1 + \frac{1}{4b^2}\right)^{(1+m_R)/2}$$

$$\lambda_{sz} = n_{sz}\, R_{ao}^{m_{sz}}\left(1 + \frac{1}{4b^2}\right)^{(1+m_{sz})/2} \tag{15}$$

$$\lambda_{s\theta} = n_{s\theta}\, R_{ao}^{m_{s\theta}}\left(1 + \frac{1}{4b^2}\right)^{(1+m_{s\theta})/2}$$

The solution of the zeroth order equations define the steady state leakage and the development of the circumferential velocity $u_{\theta o}(z)$ due to wall shear. In general the coupled and nonlinear equations have to be solved iteratively to determine the

leakage flow corresponding to a specified pressure drop. A leakage coefficient C_d can be introduced for the leakage/pressure drop relationship

$$\Delta p_o = C_d \frac{\rho}{2} \bar{V}^2 \tag{16a}$$

In formula (16a) the pressure drop at the entrance

$$\Delta p_o' = \frac{1+\xi}{(1+q)^2} \frac{\rho}{2} \bar{V}^2 \tag{16b}$$

is included. For the special case of a constant clearance seal without fluid rotation we obtain the simple relation

$$\frac{\partial p_o}{\partial z} = -(\sigma_R + \sigma_{sz}) \frac{\rho}{2} \bar{V}^2 \tag{17}$$

which can be used to determine the empirical coefficients n_R, m_R, n_{sz}, m_{sz}

First order equations

The first order equations describe the pressure and flow conditions due to a small seal motion about the centered position. Their derivation is relatively extensive, therefore we mention only some important steps in the solution procedure, following again references 1,2. To find results for the first order quantities u_{z1}, $u_{\Theta 1}$, p_1, the time and Θ-dependency is eliminated by the assumption of a harmonic pressure and velocity distribution in circumferential direction and by introducing a circular harmonic seal motion with the relative radius $r_o = R_o/\bar{C}$ and the frequency Ω. In this way the first order equations are reduced to a system of three coupled, complex ordinary differential equations for the complex unknowns u_{z1}, $u_{\Theta 1}$ and p_1, which now depend only on the axial coordinate z.

$$\frac{\partial}{\partial z} \begin{Bmatrix} u_{z1} \\ u_{\Theta 1} \\ p_1 \end{Bmatrix} + \begin{bmatrix} a_{11} & a_{12} & a_{13} \\ a_{21} & a_{22} & a_{23} \\ a_{31} & a_{32} & a_{33} \end{bmatrix} \begin{Bmatrix} u_{z1} \\ u_{\Theta 1} \\ p_1 \end{Bmatrix} = \left(\frac{r_o}{\varepsilon}\right) \begin{Bmatrix} g_1 \\ g_2 \\ g_2 \end{Bmatrix} \tag{18}$$

The 3x3-matrix A has the following elements

$$a_{11} = -2q/f \quad ; \quad a_{12} = -j\,\omega T\, f^*/f \quad ; \quad a_{13} = 0$$

$$a_{21} = f^* A_{3\Theta} \quad ; \quad a_{22} = f^*(A_{2\Theta} + j\Gamma T) \quad ; \quad a_{23} = -jf^* b(L/R)$$

$$a_{31} = A_{3z} + 2q/f^2 + j\Gamma T; \quad a_{32} = A_{2z} + j\omega T f^*/f^2 + j(L/R)H_R^*/(bf^2); \quad a_{33} = 0$$

with $\Gamma = \Omega - \omega u_{\theta o}(z)$, $T = L/\bar{V}$

and the right hand sight consists of

$$g_1 = 2q/f^3 + j\Gamma T/f$$

$$g_2 = -f^* A_{1\theta}$$

$$g_3 = -(A_{1z} + 2q/f^4 + j\Gamma T/f^2)$$

The parameters $A_{1\theta}$, $A_{2\theta}$, $A_{3\theta}$, A_{1z}, A_{2z}, A_{3z} are expressed in Appendix B.

With the boundary conditions of ref. 1 the equations (18) can be solved and yield the solution for the velocity and pressure field of the form

$$\begin{Bmatrix} u_{z1} \\ u_{\theta 1} \\ p_1 \end{Bmatrix} = \left(\frac{r_o}{\varepsilon}\right) \cdot \begin{Bmatrix} f_{1c} + j\, f_{1s} \\ f_{2c} + j\, f_{2s} \\ f_{3c} + j\, f_{3s} \end{Bmatrix} \tag{19}$$

Dynamic Coefficients

From the pressure field solution of (19) the reaction force components acting on the rotor due to the circular shaft motion can be determined by integration of the pressure along the seal and in circumferential direction. As pointed out in ref. 1 the nondimensional form of eq. (1)

$$\frac{1}{\pi R \Delta p} \cdot \begin{Bmatrix} F_x \\ F_y \end{Bmatrix} = \begin{bmatrix} \tilde{K} & \tilde{k} \\ -\tilde{k} & \tilde{K} \end{bmatrix} \begin{Bmatrix} x \\ y \end{Bmatrix} + T \begin{bmatrix} \tilde{C} & \tilde{c} \\ -\tilde{c} & \tilde{C} \end{bmatrix} \begin{Bmatrix} \dot{x} \\ \dot{y} \end{Bmatrix} + T^2 \begin{bmatrix} \tilde{M} & \tilde{m} \\ -\tilde{m} & \tilde{M} \end{bmatrix} \begin{Bmatrix} \ddot{x} \\ \ddot{y} \end{Bmatrix} \tag{20}$$

can be used in the definition for the radial and circumferential components of the reaction force

$$-\frac{F_r(\Omega T)}{\pi R \Delta p R_o} = \tilde{K} + \tilde{c}\,(\Omega T) - \tilde{M}\,(\Omega T)^2 = \frac{2}{C_d}\left(\frac{L}{\bar{C}}\right) \int_o^1 f_{3c}(z)\, dz$$

$$\frac{F_\theta(\Omega T)}{\pi R \Delta p R_o} = \tilde{k} - \tilde{C}\,(\Omega T) - \tilde{m}\,(\Omega T)^2 = \frac{-2}{C_d}\left(\frac{L}{\bar{C}}\right) \int_o^1 f_{3s}(z)\, dz \tag{21}$$

Finally the dynamic seal coefficients K, k, C, c, M, m can be found by a least square curve-fit-procedure applied to the right hand side of equation (21).

Applicability of the derived equations

The presented equations can be applied for smooth as well as grooved seals. Furthermore it is possible to investigate constant clearance and tapered seals. All equations are expressed in a form corresponding to prior derivation from Childs (ref. 1,2). Therefore it is easy to reduce the general form into simpler expressions and to compare them with prior equations. In the special case of a smooth constant clearance seal it follows $H_R = H_R^* = 0$; $H = H^*$; $n_R = n_{sz} = n_{s\Theta}$; $m_R = m_{sz} = m_{s\Theta}$; $C_s = C''_s = 1$, $q = 0$ and $h_o = 1$.
All further parameters, especially those defined in the Appendix are changing for this special case and the resultant equations coincide with the equations in ref. 1.

THEORETICAL AND EXPERIMENTAL RESULTS FOR SMOOTH AND GROOVED SEALS

The objective of the theoretical and experimental investigations is to check the usefulness of the developed model for grooved seals. For this task predicted and measured dynamic coefficients for grooved seals are compared. It is of further interest to point out differences of leakage and rotordynamic coefficients for smooth and grooved seals.

Geometry of the Test-Seals

The two seals which have been investigated are shown in fig. 9. Seal ① is a smooth constant clearance seal without any grooves, seal ② has eight parallel grooves in the stator. The rotor elements are considered to be smooth. Both seals have the following data: radius R = 23,5 mm, length L = 23,5 mm, constant clearance $\bar{C}$ = 0,2 mm. For the grooved seal the groove depth is H_R = 0,5 mm with L_G = 0,7 mm and L_L = 1,5 mm.

Test Rig for Seal Investigations

With the test rig shown in fig. 10 the leakage flow as well as the dynamic seal coefficients can be determined by measurements. The cross section shows two seal inserts integrated symmetrically in a very rigid housing. A stiff shaft, driven by an ac-motor, rotates inside the housing and acts as the second part of the seal. The housing is flexibly supported by eight beamlike springs and therefore a pure lateral motion relative to the shaft is specified. In the operating condition water with 30°C is entering the housing in the center, flows through the two test seals and is exiting the housing at both ends.

To characterize the fluid state several pressure and temperature pickups are distributed at the test apparatus. The fluid velocity, determined from the mass flow rate, was measured in the supply line. The housing can be excited by test forces, which are measured by a force transducer. To detect the resultant motion of the housing relative to the shaft eddy current-pickups were used.

For the steady-state leakage measurement the housing is fixed in a centered position and the mass flow rate and the pressure drop are taken by measurements. With this test data and additional informations concerning the fluid the leakage flow and the empirical turbulence coefficients can be found.

The experimental determination of the seal dynamic coefficients works with a parameter identification procedure. In the measurement step test forces are applied to the housing in radial direction and with the measured relative motions between the two seal surfaces mobility frequency response functions can be calculated by Fast Fourier Transformation. Corresponding frequency response curves of a seal test rig-model are fitted to the measured functions by variation of the seal dynamic coefficients. The identification procedure is described in more detail in ref. 4,5.

Leakage Performance

To compare the leakage flow of different seal stators the leakage coefficient C_L is defined as follows

$$\dot{Q} = C_L \, 2\pi R^2 \sqrt{\frac{2\Delta p_o}{\rho}} \tag{22}$$

$\dot{Q}$ is the volumetric steady state flow rate measured at the test rig and Δp the corresponding pressure drop. C_L is a nondimensional relative measure of the leakage expected trough seals with the same radius. Fig. 11 illustrates measured values C_L for the two seals without grooves and with grooves. The grooved seal ② has a leakage coefficient, which is about 15 % lower than that of seal ① without grooves. Both leakage coefficients increase slightly with the pressure drop Δp.

Empirical Turbulence Coefficients

In the described analysis the friction factors λ_R, λ_{sz}, $\lambda_{s\Theta}$ were characterized in terms of the empirical turbulence coefficients (eq. 15). These empirical coefficients have to be determined from static test data before a theoretical prediction for the seal dynamic coefficients is possible. Leakage rates and pressure gradients are measured for this task. The steady state axial pressure gradient is described by eq. (17)

$$\frac{\partial p_o}{\partial z} = - (\sigma_R + \sigma_{sz}) \frac{\rho}{2} \bar{V}^2 \tag{17}$$

With the measured pressure gradient, the velocity $\bar{V}$ and the density ρ the combined σ-values in parantheses can be calculated. We start with the smooth seal configuration and suppose that σ_R can be applied for both the smooth rotor and the smooth stator. From eq. (17) we obtain $2 \cdot \sigma_R$ and the friction factor λ_R, respectively. The second test is carried out with the smooth rotor and the grooved stator. From the measured quantities for this case first of all only the combined friction factor $(\sigma_R + \sigma_{sz})$ is known. With the value σ_R from the first test σ_{sz} and the corresponding λ_{sz} can be calculated. Fig. 12 shows the two friction factor λ_R and λ_{sz} in dependence the axial Reynolds number R_{ao}. The grooved seal ② has approximately the double friction factor compared to the smooth stator of seal ① .

From the λ versus R_{ao} data the empirical turbulence coefficients n_R, m_R, n_{sz}, m_{sz} are calculated with a least square procedure, based on equations (15). The following values were obtained (fig. 14):

$$n_R = 0{,}062 \quad ; \quad m_R = -0{,}22$$
$$n_{sz} = 0{,}058 \quad ; \quad m_{sz} = -0{,}13 \qquad (23)$$

Concerning the values $n_{s\Theta}$, $m_{s\Theta}$, we assume, that the smooth surface constants are relevant.

Dynamic Coefficients, Influence of the Groove depth

With the presented analysis we can now calculate the dynamic seal coefficients. The numerical procedure is applied to determine especially the stiffness and damping coefficients K, k, C, c for seal ② in dependence of the rotational speed and the average groove depth. The axial Reynolds number R_{ao} is kept constant in this investigation. Besides the seal geometry (fig. 9) further input data are as follows:

Fluid data for water with 30°C
Axial average velocity $\bar{V}$ = 16,46 m/sec
Entry swirl $U_{\Theta o}$ = 0,2 $R\omega$
Inlet pressure loss ξ = 0,5

Describing the friction behavior, the empirical coefficients from (23) are used (fig. 14).

To point out the influence of the groove depth, different values of H_R^* are assumed (figs. 13,14). Taking the average depth from a geometrical approximation (sum of the upper areas equal the sum of the lower areas) we obtain $H_R^* \cong 0{,}1$ mm. The selected values for the calculations are $H_R^* = 0;\ 0{,}1;\ 0{,}2$ mm. Note that the empirical constants are held constant in this investigation.

Fig. 13 illustrates that the direct stiffness and damping as well as the cross coupled stiffness are reduced by H_R^*, there is a weak influence to the cross coupled damping. An increase of H_R^* from 0 to 0,2 mm reduces K about 50 % and C about 37 %, respectively.

In Fig. 14 the direct stiffness K and the direct damping C are compared for the two seal types ① and ② . All presented values are related to the coefficients K and C of seal ① without grooves. The results correspond to R_{ao} = 8419 and a rotational speed 4000 rpm. All other data are the same as in the example before. Starting with the reference seal ① with empirical constants for smooth surfaces the stiffness ratio as well as the damping ratio are equal to 1 by definition. Seal ② with grooves has other constants (fig. 14). If we consider only this influence (change in friction) and keep the average groove depth constant ($H_R^* = 0$), direct stiffness as well as damping increase to 1,12 and 1,19 respectively. Taking now the empirical values of seal ② constant, an increase of H_R^* reduces both stiffness and damping, as was shown already in fig. 13. If we compare with corresponding measurement results, we recognize that the calculation with $H_R^* = 0{,}1$ mm yields good results for stiffness but 15 % too high values for the damping.

Dynamic Coefficients, Comparison of Test Results and Theoretical Results

As described before the dynamic seal coefficients can be measured at the seal test rig. For one working condition with constant rotational speed, axial velocity and constant fluid temperature four frequency response functions are measured by exciting the dynamic seal test rig and picking up the response in the two directions. A computer takes over the measured data and calculates the dynamic seal coefficients by means of a least square identification procedure (references 4,5). Several measurements were carried out for different rotational speeds but constant axial Reynolds number R_{ao} and fluid temperature. Fig. 15 illustrates for the two seals with and without grooves the identified stiffness and damping coefficients versus the rotational speed. The test results show, that neither the direct coefficients nor the cross coupled coefficients are equal in amount, as expected from theory (eq. 1). Each of the two coefficients, which should be equal in magnitude, are shown in the diagram as found out by the identification process. The scatter of the measurement points is very different. The added mass terms are much higher than predicted by theory. They are not presented in the diagram.

The fitting curves show the tendency as expected from theory, a slightly parabolic decrease of K with the rotational speed, constant direct damping and a linear increase with the rotational speed for the cross coupled terms k and c.

Seal ① without grooves has higher direct stiffness and damping terms compared to seal ② with grooves. The cross coupled stiffness of seal ① is also greater than of seal ② . There is no clear difference in the cross coupled damping values. Basicly, the different measurement results for the two seal types show the expected influence of the grooves (see also fig. 13), reducing especially K, C and k.

In fig. 16 the identified stiffness and damping coefficients of seal ② are refered to the corresponding predictions from the grooved seal model. There are two parameters in the model, which can be changed slightly, to obtain a better correlation between measured and theoretical results: the average groove depth H_R^* and fluid entry swirl at the seal entrance. It was found, that values for the entry swirl between $U_{\Theta o} = 0{,}1\ R\omega$ for low rotational speeds and $U_{\Theta o} = 0{,}3\ R\omega$ for higher rotational speeds and a average groove depth of $H_R^* = 0{,}1$ mm were best suited to fit the theoretical values to the test results. The predicted direct stiffnesses are slightly lower, the direct damping values about 20 % higher than the measured quantities.

The influence of the axial Reynolds number for a constant rotational speed of 4500 rpm is pointed out in fig. 17. Measured as well as predicted parameters show the similar trend for the different seal coefficients. K is increasing in a parabolic curve, C depends linear on the Reynolds number and the cross coupled terms k and c behave indifferent.

Finally in fig. 18 the seal model predictions for the two seal types are compared, in accordance to the measurement results in fig. 15. The results are as follows, an expected decrease of both stiffness coefficients from seal ① to seal ② but a weak difference of the damping parameters for the two seals.

CONCLUDING REMARKS

A theoretical model, based on Childs finite length solution, is presented to determine rotordynamic coefficients and the leakage flow of seals with parallel grooves in the stator. Calculated and measured stiffness and damping values for the investigated seal with eight grooves show, that the developed model is useful for the prediction of this seal type.

Concerning the pump efficiency seals with grooves have the advantage of a lower leakage flow compared to the smooth seal. But the direct and cross coupled stiffness coefficients as well as the direct damping are reduced in the grooved seal configuration. This has to be considered when rotordynamic problems are important.

APPENDIX A: COMPLETE BULK FLOW EQUATIONS

$$-H\frac{\partial p}{\partial z} = \frac{n_R}{2}\rho U_z^2\left(\frac{2HU_z}{\nu}\right)^{m_R}\cdot\left\{1+\left(\frac{U_\theta - R\omega}{U_z}\right)^2\right\}^{(1+m_R)/2} +$$

$$+ C_s'\,\frac{n_{sz}}{2}\rho U_z^2\left(\frac{2HU_z}{\nu}\right)^{m_{sz}}\cdot\left\{1+\left(\frac{U_\theta}{U_z}\right)^2\right\}^{(1+m_{sz})/2}$$

$$+ \rho H\left(\frac{\partial U_z}{\partial t} + U_z\frac{\partial U_z}{\partial z} + U_\theta\cdot\frac{\partial U_z}{R\,\partial\theta}\right) - \rho H_R^* U_z\,\frac{1}{R}\frac{\partial U_\theta}{\partial\theta}$$

$$-\frac{H^*}{R}\frac{\partial p}{\partial\theta} = \frac{n_R}{2}\rho\left(\frac{H^*}{H}\right)^{m_R} U_z(U_\theta - R\omega)\left(\frac{2HU_z}{\nu}\right)^{m_R}\left\{1+\left(\frac{U_\theta - R\omega}{U_z}\right)^2\right\}^{(1+m_R)/2}$$

$$+ C_s''\,\frac{n_{s\theta}}{2}\rho\cdot\left(\frac{H^*}{H}\right)^{m_{s\theta}} U_z U_\theta\left(\frac{2HU_z}{\nu}\right)^{m_{s\theta}}\left\{1+\left(\frac{U_\theta}{U_z}\right)^2\right\}^{(1+m_{s\theta})/2}$$

$$+ \rho H^*\left(\frac{\partial U_\theta}{\partial t} + \frac{U_\theta}{R}\frac{\partial U_\theta}{\partial\theta} + U_z\frac{\partial U_\theta}{\partial z}\right) - \rho H_R^* U_z\frac{\partial U_\theta}{\partial z}$$

$$\frac{\partial H}{\partial t} + \frac{1}{R}\frac{\partial(HU_\theta)}{\partial\theta} + \frac{\partial(HU_z)}{\partial z} + \frac{1}{R}H_R^*\cdot\frac{\partial U_\theta}{\partial\theta} = 0$$

$$C_s' = \sqrt{\frac{U_z^2}{U_z^2+U_\theta^2} + \left(\frac{n_{s\theta}}{n_{sz}}\right)^2\frac{H^{*\,2m_{s\theta}}}{H^{2m_{sz}}}\left(\frac{2}{\nu}\right)^{2(m_{s\theta}-m_{sz})}\left(U_z^2+U_\theta^2\right)^{m_{s\theta}-m_{sz}-1}\cdot U_\theta^2}$$

$$C_s'' = \sqrt{\frac{U_\theta^2}{U_\theta^2+U_z^2} + \left(\frac{n_{sz}}{n_{s\theta}}\right)^2\left(\frac{2}{\nu}\right)^{2m_{sz}-2m_{s\theta}}\cdot\frac{H^{2m_{sz}}}{H^{*2m_{s\theta}}}\left(U_z^2+U_\theta^2\right)^{m_{sz}-m_{s\theta}-1}\cdot U_z^2}$$

APPENDIX B: PERTURBATION COEFFICIENTS

$$B_{sz}\, a_{osz} = \left\{ 1 + (u_{\theta o}/b u_{zo})^2 \right\}^{(1+m_{sz})/2} ; \quad B_{sz} = (1 + 1/4b^2)^{(1+m_{sz})/2}$$

$$B_{s\theta}\, a_{os\theta} = \left\{ 1 + (u_{\theta o}/b u_{zo})^2 \right\}^{(1+m_{s\theta})/2} ; \quad B_{s\theta} = (1 + 1/4b^2)^{(1+m_{s\theta})/2}$$

$$B_R\, a_{oR} = \left\{ 1 + ([v_{\theta o}-1]/b u_{zo})^2 \right\}^{(1+m_R)/2} ; \quad B_R = (1 + 1/4b^2)^{(1+m_R)/2}$$

$$A_{1\theta} = -\left\{ \alpha_1 \left[(m_R - 1)(u_{\theta o} - 1) \frac{1}{h_o^*} \right] + \alpha_2 \left[v_{\theta o} \left((m_{s\theta} - 1) \frac{1}{h_o} + D a_3 + (1 - m_{s\theta}) \frac{H_R^*}{h_o h_o^*} \right) \right] + \frac{u_{zo} H_R^*}{h_o^{*2}} \frac{\partial u_{\theta o}}{\partial z} \right\}$$

$$A_{2\theta} = \left\{ \alpha_1 \left[1 + (u_{\theta o} - 1)(m_R + 1) \frac{u_{\theta o} - 1}{b^2 u_{zo}^2 + (u_{\theta o} - 1)^2} \right] + \alpha_2 \left[1 + u_{\theta o} D a_2 + \frac{(m_{s\theta} + 1) u_{\theta o}^2}{b^2 u_{zo}^2 + u_{\theta o}^2} \right] \right\}$$

$$A_{3\theta} = \left\{ \alpha_1 \left[(u_{\theta o} - 1)(m_R + 1) \frac{b^2 u_{zo}}{b^2 u_{zo}^2 + (u_{\theta o} - 1)^2} \right] + \alpha_2 \left[u_{\theta o} \left(\frac{(m_{s\theta} + 1) b^2 u_{zo}}{b^2 u_{zo}^2 + u_{\theta o}^2} + D a_1 \right) \right] + \frac{\partial u_{\theta o}}{\partial z} \frac{h_o}{h_o^*} \right\}$$

$$A_{1z} = -\left\{ \alpha_3 \frac{u_{zo}}{h_o} (m_R - 1) + \alpha_4 \left(u_{zo} (m_{sz} - 1) \cdot \frac{1}{h_o} + D e_3\, u_{zo} \right) \right\}$$

$$A_{2z} = \left\{ \alpha_3\, u_{zo} (m_R + 1) \frac{u_{\theta o} - 1}{b^2 u_{zo}^2 + (u_{\theta o} - 1)^2} + \alpha_4 \left(\frac{u_{zo} (m_{sz} + 1) u_{\theta o}}{b^2 u_{zo}^2 + (u_{\theta o})^2} + D e_2\, u_{zo} \right) \right\}$$

$$A_{3z} = \left\{ \alpha_3 \left(1 + \frac{u_{zo} (m_R + 1) b^2 u_{zo}}{b^2 u_{zo}^2 + (u_{\theta o} - 1)^2} \right) + \alpha_4 \left(1 + \frac{u_{zo} (m_{sz} + 1) b^2 u_{zo}}{b^2 u_{zo}^2 + u_{\theta o}^2} + D e_1\, u_{zo} \right) + \frac{2q}{f^2} \right\}$$

$$\alpha_1 = \left(\frac{h_o^*}{h_o} \right)^{m_R - 1} \cdot \alpha_3 ; \quad \alpha_3 = \frac{1}{2 f^2}\, b_R\, a_{oR} ;$$

$$\alpha_2 = \frac{1}{2 f^2} \left(\frac{h_o^*}{h_o} \right)^{m_{s\theta} - 1} b_{s\theta}\, a_{os\theta}\, D a ; \quad \alpha_4 = \frac{1}{2 f^2}\, b_{sz}\, a_{osz}\, D e ;$$

The parameters D_e, D_a, D_{ei}, D_{ai} are very extensive and therefore not presented. If desired, they can be obtained by the authors.

REFERENCES

1. Childs, D.W., "Finite Length Solutions for Rotordynamic Coefficients of Turbulent Annular Seals", Journal of Lubrication Technology, ASME-Paper No. 82-Lub 42, 1982

2. Childs, D.W. and Chang-Ho Kim, "Analysis and Testing for Rotordynamic Coefficients of Turbulent Annular Seals Different, Directionally Homogeneous Surface-Roughness Treatment for Rotor and Stator Elements", Journal of Tribology, ASME-Paper No. 84-Trib-31, 1985

3. Childs, D.W. and Dressmann J.B., "Testing of Turbulent Seals for Rotordynamic Coefficients", NASA-Conference Publication 2250, Rotordynamic Instability Problems of High Performance Turbomachinery, Proc. of a workshop 1982, pp. 157-171, 1982

4. Nordmann, R. and Maßmann, H., "Identification of Dynamic Coefficients of Annular Turbulent Seals", NASA Conference Publication 2338, Rotordynamic Instability Problems in High Performance Turbomachinery, Proc. of a workshop 1984, pp. 295-311, 1984

5. Maßmann, H. and Nordmann, R., "Some New Results Concerning the Dynamic Behavior of Annular Turbulent Seals", NASA-Conference Publication 2409, Instability in Rotating Machinery, Proceedings of a Symposium held in Carson City, pp. 179-194, 1985

6. Black, H.F. and Cochrane, E.A., "Leakage and Hybrid Bearing Properties of Serrated Seals in Centrifugal Pumps", Paper G5, 6-th International Conference on Fluid Sealing, Munich 1973, pp. G5-61 - G5-70

7. Chang-Ho Kim and Childs D.W., "Analysis and Testing for Rotordynamic Coefficients of Grooved Turbulent Annular Seals", Turbomachinery Report Texas A&M University, June 1985.

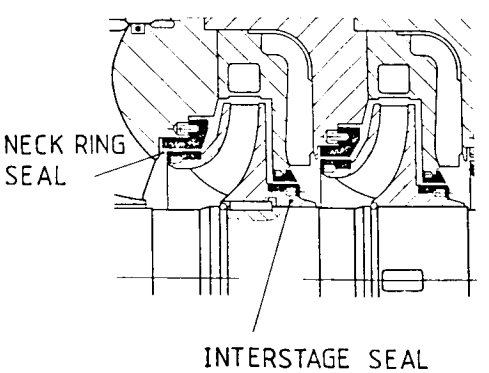

Figure 1. - Seal types in turbopumps

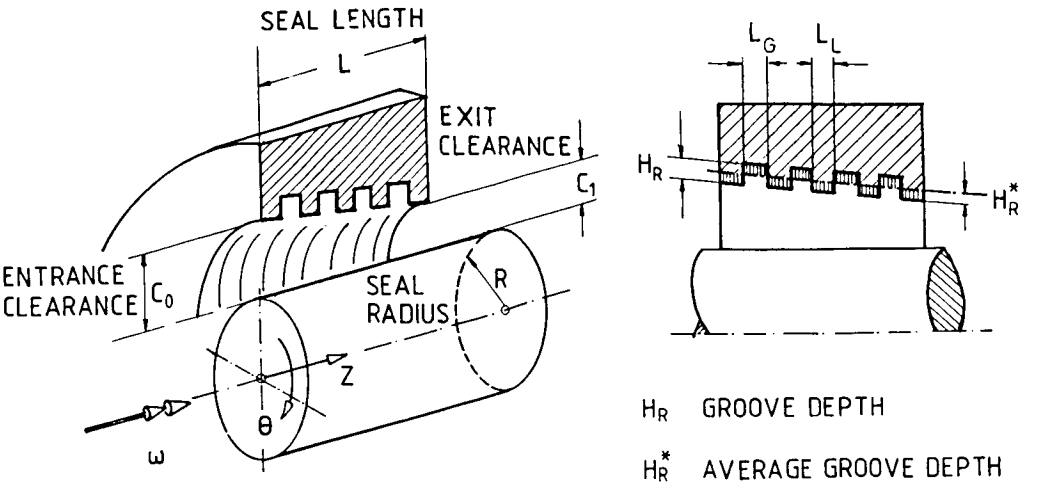

Figure 2. - Seal with parallel grooves in the stator

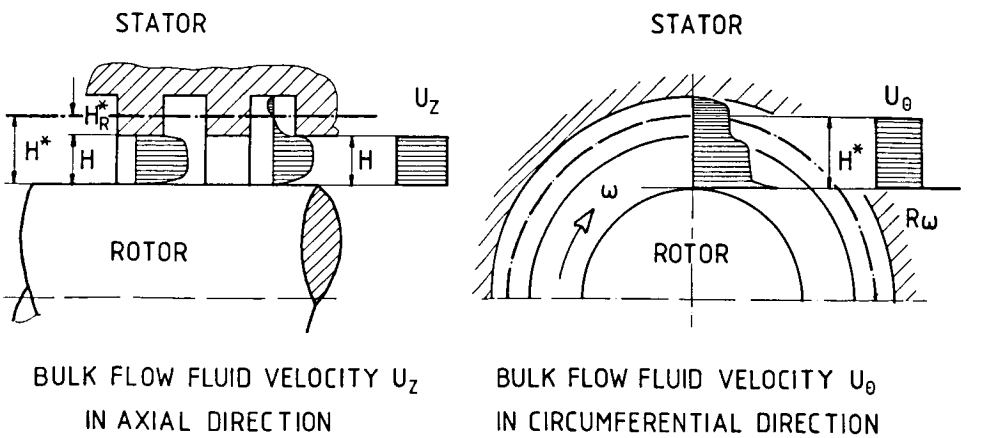

Figure 3. - Bulk flow velocities

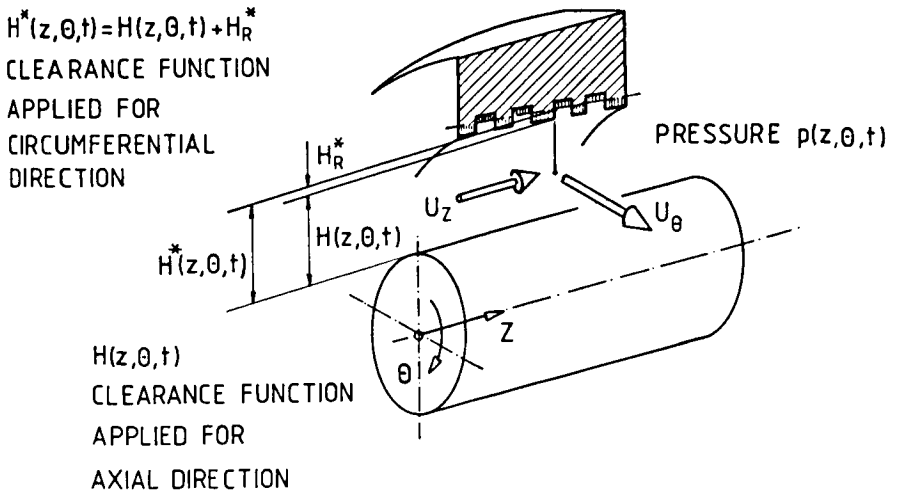

Figure 4. - Variables of the bulk flow model

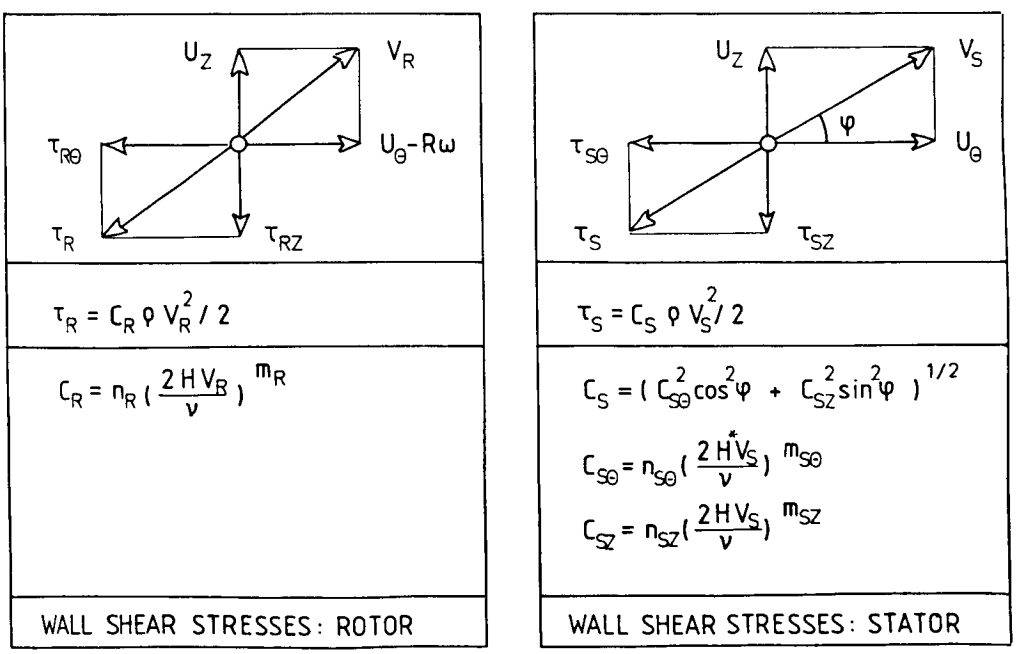

Figure 5. - Wall shear stresses

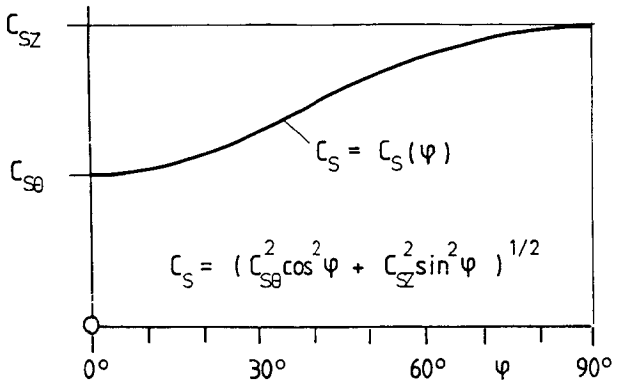

Figure 6. - Stator friction factor in dependence of the flow angle

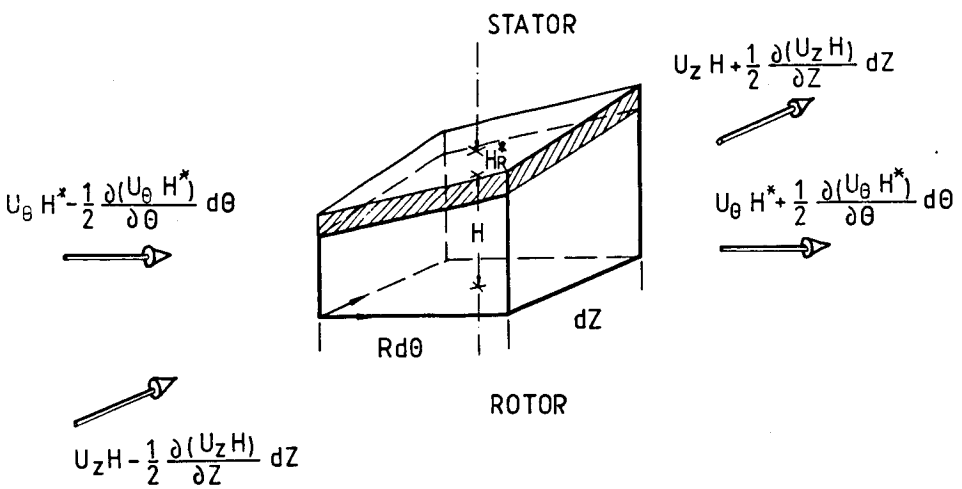

Figure 7. - Bulk flow velocities at differential element

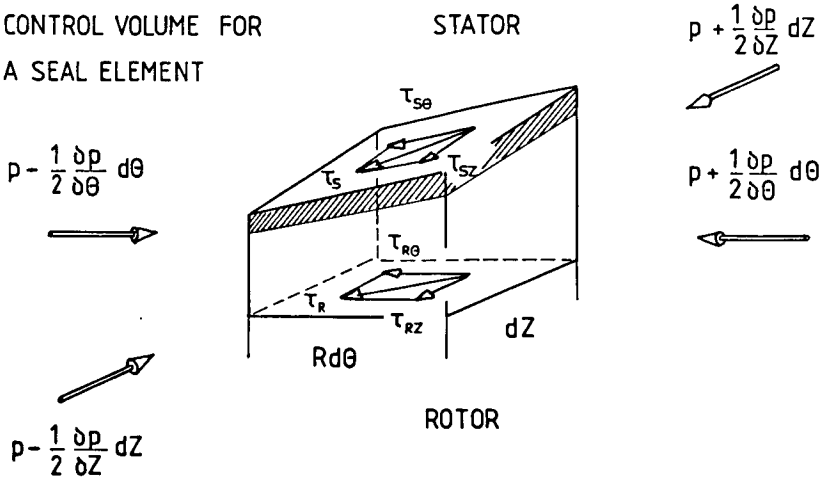

Figure 8. - Control volume for a seal element with pressure and shear stresses

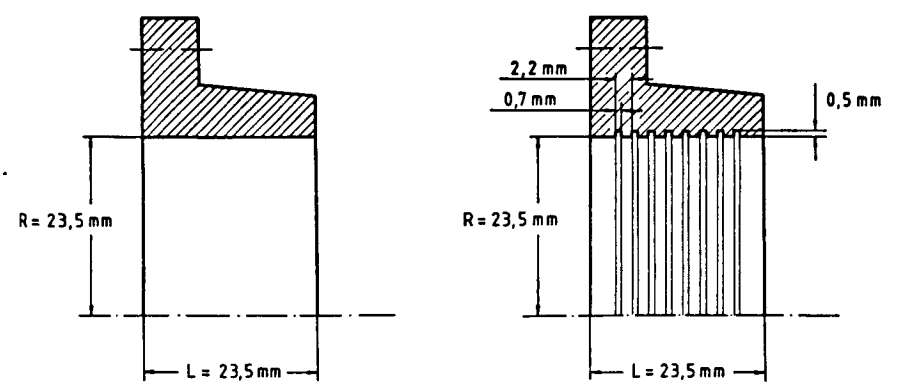

STATOR OF SEAL ① WITHOUT PARALLEL GROOVES

STATOR OF SEAL ② WITH 8 PARALLEL GROOVES

Figure 9. - Investigated seals with and without grooves

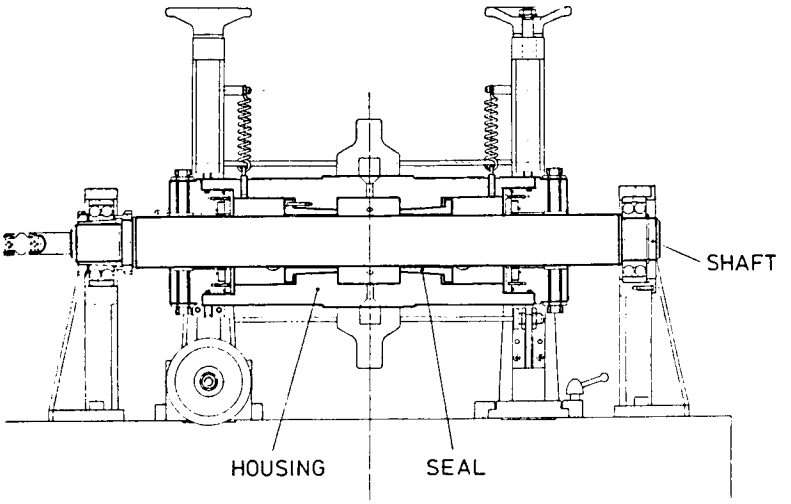

Figure 10. - Seal test rig

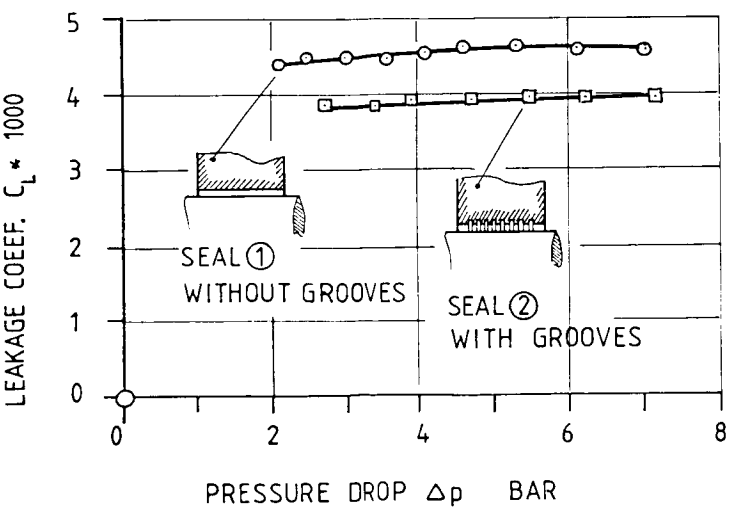

Figure 11. - Leakage coefficients for seal 1 and seal 2

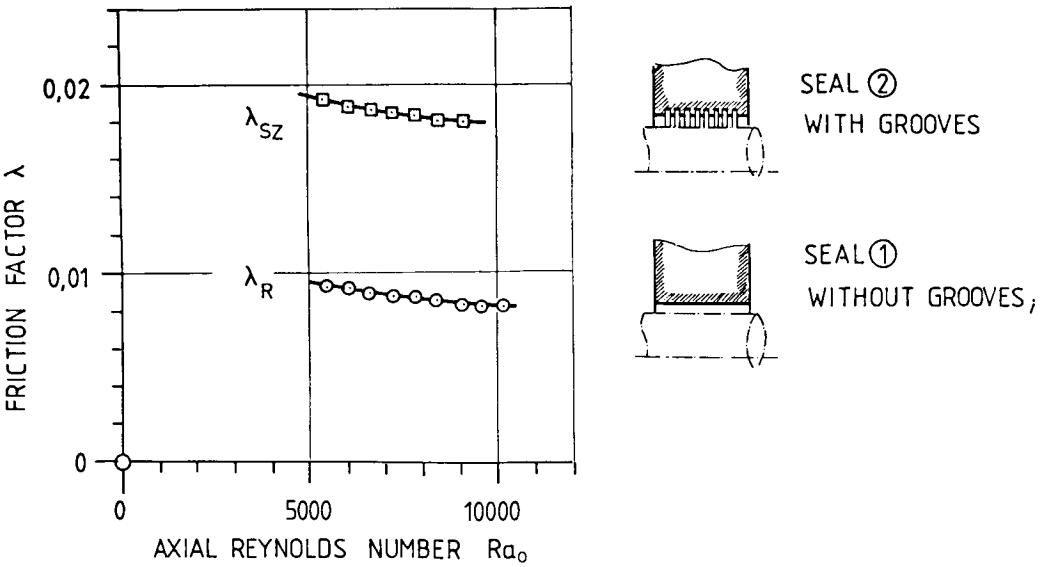

Figure 12. - Friction factors for the stators of seal 1 and seal 2

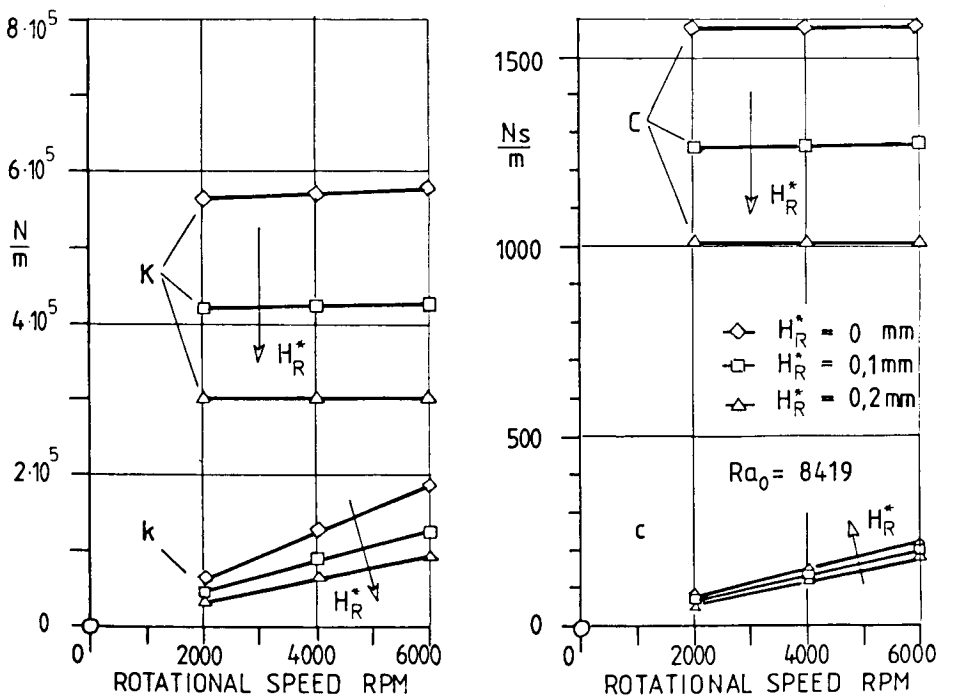

Figure 13. - Calculated stiffness and damping coefficients of a grooved seal in dependence of the rotational speed and the average groove depth

	SEAL 1	SEAL 2 WITH GROOVES			MEASUREMENT
	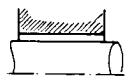	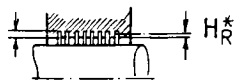			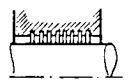
H_R^* mm	$H_R^* = 0$	$H_R^* = 0$	$H_R^* = 0{,}1$	$H_R^* = 0{,}2$	$H_R^* = ?$
STIFFNESS RATIO K/K_{SEAL1}	1,00	1,12	0,83	0,60	0,86
DAMPING RATIO C/C_{SEAL1}	1,00	1,19	0,96	0,76	0,83
EMPIRICAL CONSTANTS	$n_R = n_{S\theta} = n_{SZ} = 0{,}062$	$n_R = n_{S\theta} = 0{,}062$; $n_{SZ} = 0{,}058$			
	$m_R = m_{S\theta} = m_{SZ} = -0{,}22$	$m_R = m_{S\theta} = -0{,}22$; $m_{SZ} = -0{,}13$			

Figure 14. - Comparison of calculated and measured direct stiffness and damping coefficients for seals 1 and 2

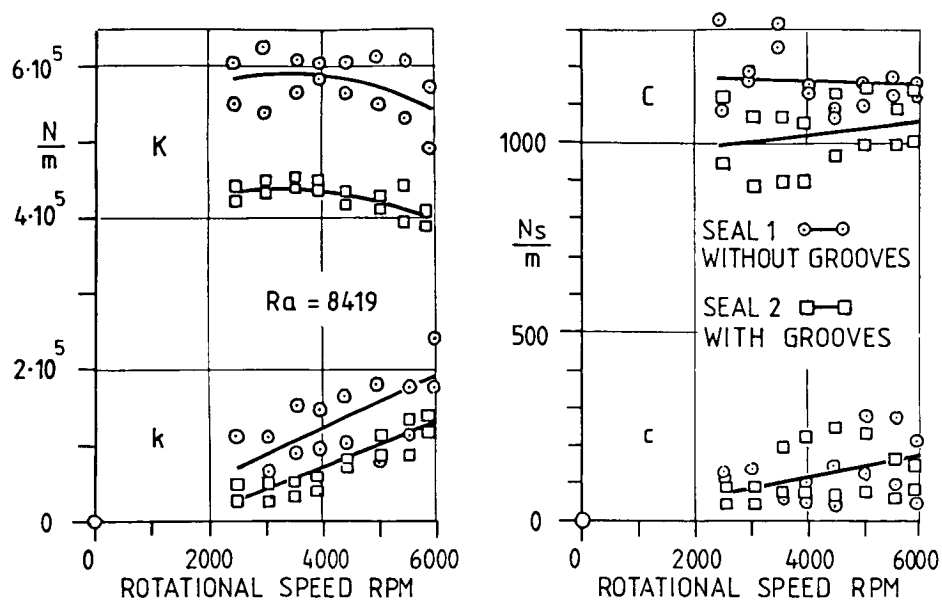

Figure 15. - Measured stiffness and damping coefficients in dependence of rotational speed for seals 1 and 2

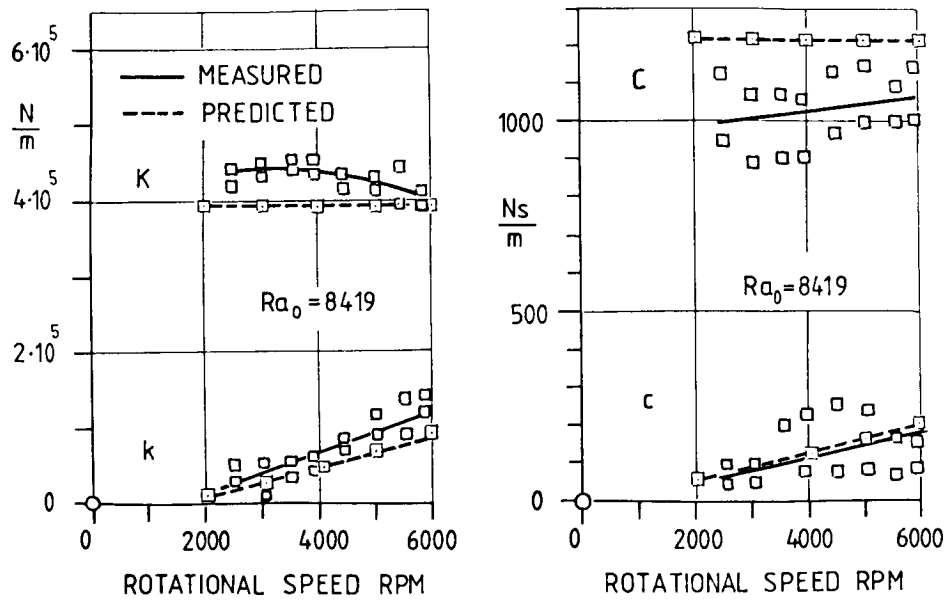

Figure 16. - Measured and predicted stiffness and damping coefficients in dependence of rotational speed for the grooved seal 2

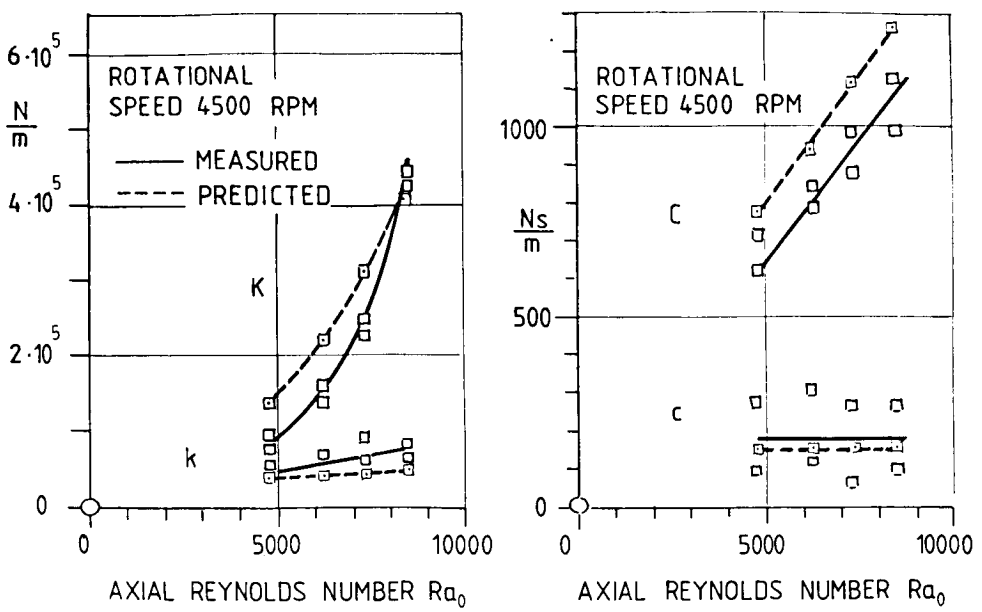

Figure 17. - Measured and predicted stiffness and damping coefficients in dependence of the axial Reynolds number for the grooved seal 2

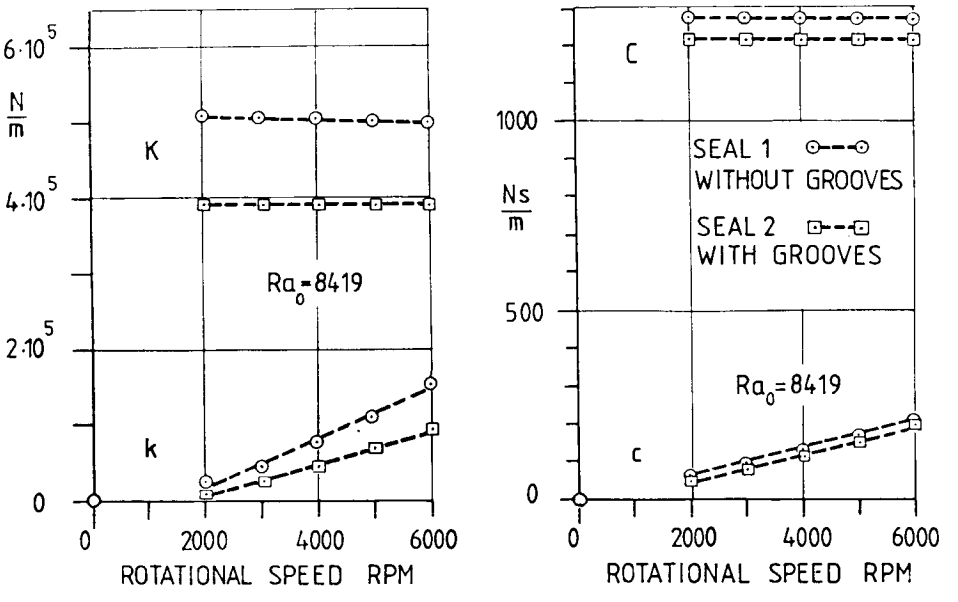

Figure 18. - Predicted stiffness and damping coefficients in dependence of rotational speed for seals 1 and 2